Supplemental Information Appendix for Measuring response functions of active materials from data

Mehdi Molaei [*,1,2,3,**], **Steven A. Redford** [*,2,3,4,**], **Wen-hung Chou** [2,3,4] **Danielle Scheff** [2,3,5] **Juan J. de Pablo** [1] **Patrick W. Oakes** [6] **Margaret L. Gardel** [1,2,3,5,**]

[1]Pritzker School of Molecular Engineering, University of Chicago, Chicago, IL 60637, U.S.A.
[2]James Franck Institute, University of Chicago, Chicago, IL 60637, U.S.A.
[3]Institute for Biophysical Dynamics, University of Chicago, Chicago, IL 60637, U.S.A.
[4]Graduate Program in Biophysical Sciences, University of Chicago, Chicago, IL 60637, U.S.A.
[5]Department of Physics, University of Chicago, Chicago, IL 60637, U.S.A.
[6]Department of Cell and Molecular Physiology, Stritch School of Medicine, Loyola University Chicago, Maywood, IL 60153, U.S.A.
[*] These authors contributed equally
[**]Correspondence: mehdi.molai@gmail.com, redford@uchicago.edu, gardel@uchicago.edu

SUPPLEMENTAL TEXT

General cross correlation function

In the main text we consider a simplified correlation function. Here let us consider a general version of the spatiotemporal correlation function

$$\boldsymbol{C_{pq}}(\boldsymbol{R},\tau) = \langle \boldsymbol{p}(\boldsymbol{r}_1,t)\boldsymbol{q}(\boldsymbol{r}_2,t+\tau)\delta(\boldsymbol{R}-\boldsymbol{r}_{12})\rangle_{\boldsymbol{r}_1,\boldsymbol{r}_2,t}, \tag{S1}$$

here $\boldsymbol{p}$ and $\boldsymbol{q}$ denote dynamical fields measured at time t and $t+\tau$ respectively. The relationship being queried is the tensor product between $\boldsymbol{p}$ and $\boldsymbol{q}$ at positions $\boldsymbol{r}_1$ and $\boldsymbol{r}_2$. $\boldsymbol{R}$ is a location with respect to a coordinate system with its origin at $\boldsymbol{r}_1$. In order to make this comparison meaningful for the system at large, we average over all positions $\boldsymbol{r}_2$ for each origin $\boldsymbol{r}_1$ and then take the average over observation time denoted as $\langle\rangle_{\boldsymbol{r}_1,\boldsymbol{r}_2,t}$. For simplicity we will omit subscripts and simply denote this operation as $\langle\rangle$. The role of δ is to bin the average into proper ensembles based on the spatial location $\boldsymbol{R}$. δ is a finite width delta function and sets the spatial precision of the measurement. In an ideal case this function has infinitesimal width and, δ is Kronecker delta function. $\boldsymbol{p}$ and $\boldsymbol{q}$ can either denote to same dynamic variable, as in the case of auto-correlation, or they can denote different quantities as in the case of cross-correlation. In Euclidean space, $\boldsymbol{C_{pq}}(\boldsymbol{R},\tau)$ is basically the first mode of probability of observable $\boldsymbol{q}$ at the space-time point of $\boldsymbol{R}$ and τ if we know the value of $\boldsymbol{p}$ at the origin. Note that taking the tensor product of $\boldsymbol{p}$ and $\boldsymbol{q}$ contains all of the information that might be desired from a traditional correlation function with a different product. For example, the spatial velocity-velocity correlation function $\boldsymbol{C_{v\cdot v}}(R) = \langle \boldsymbol{v}(\boldsymbol{r}_1)\cdot\boldsymbol{v}(\boldsymbol{r}_2)\delta(R-|\boldsymbol{r}_1-\boldsymbol{r}_2|)\rangle$ is the trace of equal-time auto-correlation tensor $\boldsymbol{C_{vv}}$ in which $\boldsymbol{R}$ is converted to the scalar distance R. The choice of product or the manipulation of the tensor product is one of the key choices that lend this correlation function its interpretability. The other crucial piece is the choice of the coordinate system for $\boldsymbol{R}$. Note that, both of this choices depend on the physics of the system. In the rest of this section we give one example of simplifying high rank correlation tensor related to the systems discussed in the main text as a guideline for other problems. Note that, we are only addressing linear systems here to take advantage of their superposition property.

When $\boldsymbol{p}$ is a tensor with a rank higher than zero, for example when it is a velocity vector or a stress tensor, choosing specific coordinate systems for forming conditional averaging is a crucial step. When $\boldsymbol{p}$ is a vector field, the direction of the vector is an obvious choice as describe in the text. However, consider an example where p_{ij} is a second rank tensor and q_i is a vector; therefore, $\boldsymbol{C_{pq}}$ is a third rank tensor in two dimensions. To fully resolve $\boldsymbol{C_{pq}}$ we need to construct 4 general correlation vector field of $\boldsymbol{\chi}$. One can consider various decomposition of $\boldsymbol{p}$ to form different meaningful $\boldsymbol{\chi}$. For example if $\boldsymbol{p}$ denotes a strain tensor its principle directions can be used to set up the coordinate system and its invariant can be used as scalar in the modified correlation functions. Seeking to understand how vortical, normal, and shear deformations propagate in

the active system we choose to decompose $\boldsymbol{p} = \boldsymbol{\nabla u}$ into the anisotropic symmetric traceless strain rate tensor, $S_{ij} = (\partial_i u_j + \partial_j u_i)/2 - \partial_k u_k I_{ij}/2$, the isotropic symmetric strain rate tensor $D_{ij} = \partial_k u_k I_{ij}/2$, and the circulation tensor $\Omega_{ij} = (\partial_i u_j - \partial_j u_i)/2$. Spatiotemporal correlation function for $\boldsymbol{C}_{(\boldsymbol{\nabla u})\boldsymbol{u}}$ then can be written as

$$\begin{aligned}\boldsymbol{C}_{(\boldsymbol{\nabla u})\boldsymbol{q}}(\boldsymbol{R},\tau) &= \langle[\boldsymbol{S}(\boldsymbol{r}_1,t) + \boldsymbol{D}(\boldsymbol{r}_1,t) + \boldsymbol{\Omega}(\boldsymbol{r}_1,t)]\boldsymbol{q}(\boldsymbol{r}_2,t+\tau)\delta(\boldsymbol{R}-\boldsymbol{r}_{12})\rangle \\ &= \langle \boldsymbol{S}(\boldsymbol{r}_1,t)\boldsymbol{q}(\boldsymbol{r}_2,t+\tau)\delta(\boldsymbol{R}-\boldsymbol{r}_{12})\rangle \\ &+ \langle \boldsymbol{D}(\boldsymbol{r}_1,t)\boldsymbol{q}(\boldsymbol{r}_2,t+\tau)\delta(\boldsymbol{R}-\boldsymbol{r}_{12})\rangle \\ &+ \langle \boldsymbol{\Omega}(\boldsymbol{r}_1,t)\boldsymbol{q}(\boldsymbol{r}_2,t+\tau)\delta(\boldsymbol{R}-\boldsymbol{r}_{12})\rangle.\end{aligned} \tag{S2}$$

Where each term on the right hand side can be reduced to a vector field by the treatment described in the text. Note that in two dimensions $\boldsymbol{C}_{(\boldsymbol{\nabla u})\boldsymbol{u}}$ has 8 degrees of freedom. In an isotropic system with no odd deformation field eight degree of freedoms in $\boldsymbol{C}_{(\nabla \boldsymbol{u})\boldsymbol{u}}$ reduces to 4. In the active system described in the text, $\boldsymbol{C}_{(\boldsymbol{\nabla u})\boldsymbol{u}}$ were decomposed to $\boldsymbol{\chi_S}$, $\boldsymbol{\chi}_\nu$, and $\boldsymbol{\chi}_D$. Since $\boldsymbol{S}$ is a symmetric tensor and traceless $\boldsymbol{\chi}_S(\boldsymbol{R})$ is symmetric about both X and Y axes and has two degree of freedoms. $\boldsymbol{\chi}_\nu$ only has the angular component, and $\boldsymbol{\chi}_D$ only has the radial component. Therefore, the set of modified correlation functions $\boldsymbol{\chi}_{\boldsymbol{S},\,\nu,\,D}$ fully captures the third rank correlated tensor field $\boldsymbol{C}_{(\nabla \boldsymbol{u})\boldsymbol{u}}$.

Effect of uncorrelated noise on response function

One advantage of the correlated based measurement is its ability to filter the effect of the uncorrelated noise in the measurement of the response function. To illustrate this aspect of the method, we take the displacement field of the active nematic system presented in figure 1 in the main text and superimposed it with the uncorrelated displacement fields with different strength of the noise level. The rms value of the original displacement field shown in figure 1.A is $\sim 0.2\,\mu$m. We synthetically generate three sets of noise displacement fields with normal distribution with mean value of zeros and standard deviation of 0.2, 0.6 and 1.2 µm and superimposed them on the displacement field measured by optical flow Fig. S1 (top row). The measured shear, Fig. S1(middle row) and displacement, Fig. S1(bottom row) response functions for these fields are similar to the response functions of the original field, indicating efficacy of the generalized correlated displacement measurement in revealing underlying response function of the system even in the presences of strong noise. Fig. S2 shows quantitative agreement of the response functions of the original nematic system and the synthetically generated fields. When we remove the underlying original displacement field and only keep the noise displacement field, the response function vanishes as expected, Fig. S2. Note that to remove the effect of noise in the system and to capture steady response functions sufficient number of displacement vectors should be collected in each bin until the measured average values converge, Fig. S3.

SUPPLEMENTAL FIGURES

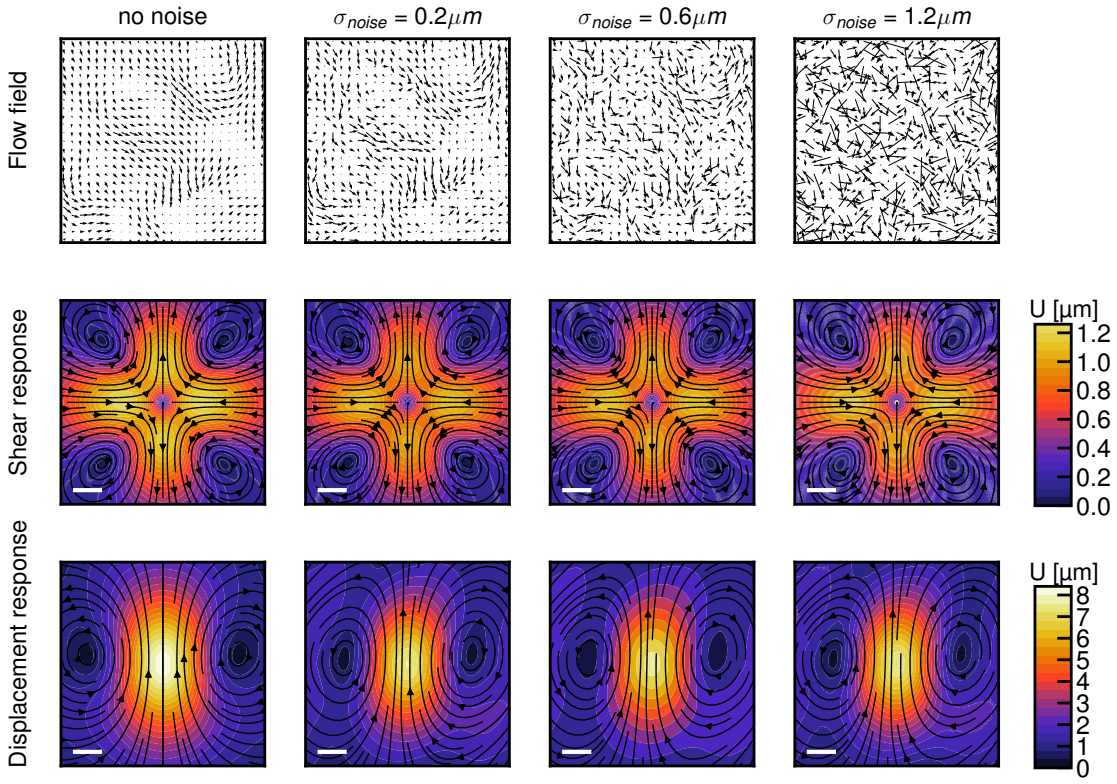

Figure S1: Response function for noisy nematic system. First column (labeled as no noise) show same velocity field and response functions of the nematic fields as shown in Figure 1 of the main text. Columns 2 to 4 show velocity field and response function for synthetically generated noisy system. top rows: Velocity field generated by superposition of the velocity field of no-noise system with random displacement fields with mean displacement of zeros and standard deviation of $\sigma_{noise} = 0.2$, 0.6, and 1.2 μm. Second and third row: Equal time shear and displacement response of the fields shown in the top row. Streamlines indicate the direction of the resulting response function and color indicates the magnitude; scale bars are 5 μm.

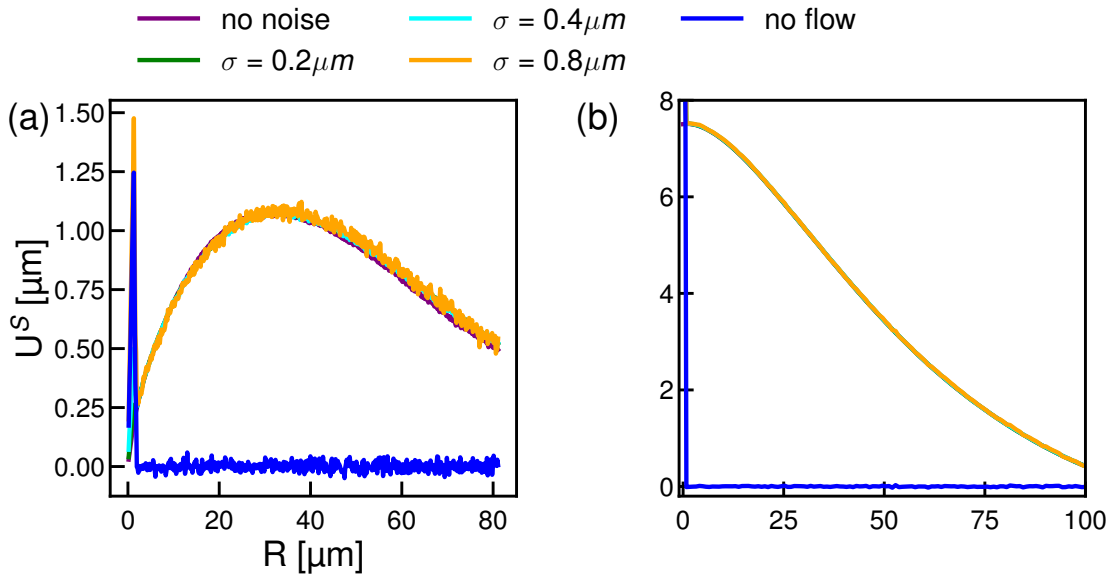

Figure S2: Profile of shear and displacement response functions for noisy systems. One dimensional profiles are constructed by tracing measured fields shown in Fig. S1 along the Y axis, with an additional profile for the pure uncorrelated noisy field without underlying correlated displacement field.

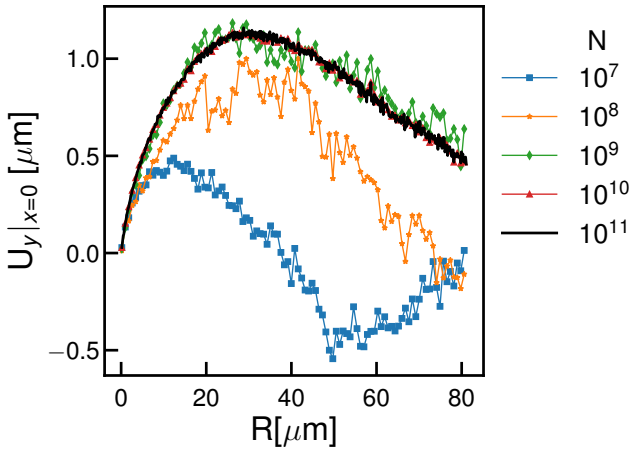

Figure S3: Profile of response function measured using different number of points Shear response profiles for nematics from Fig 1 constructed from variously sub-sampled data show the sensitivity of the measured response function to the number of data points. In order to remove effect of uncorrelated noise from the underlying physical response sufficient data should be collected until the response function converges to a final profile.

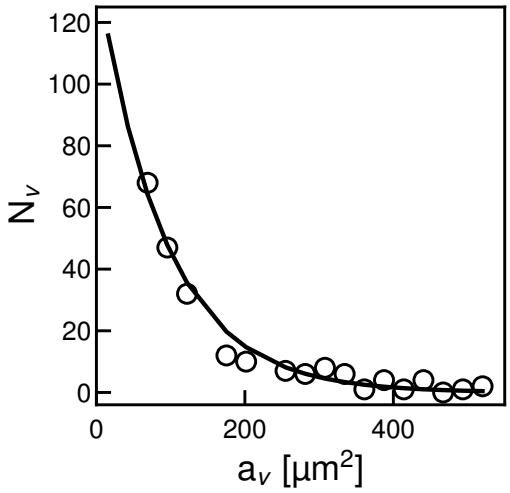

Figure S4: Statistical analysis of vortex size. Number of vortexes with different sizes, open circles, in the 2D active nematics of the short actin filaments studied in figure 1 in the main text. The solid line is an exponential fit to the data. The size of the field of view limits the range of vortex size measurement.

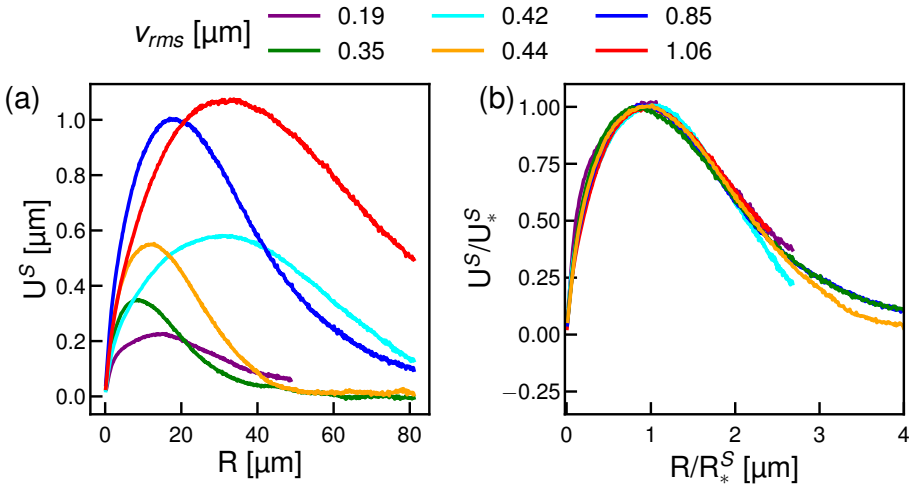

Figure S5: Scaling behavior of active nematics: Because critical scales are model-free and unambiguous they easily allow for comparisons between experimental conditions. a) Correlated deformation profiles of nematics with different rms displacement over $\Delta t = 2\,\mathrm{s}$. b) Correlated deformation shown in (a) normalized with characteristic displacement scales U^S_* as a function of distance normalized with charactetic length scale R^S_*.

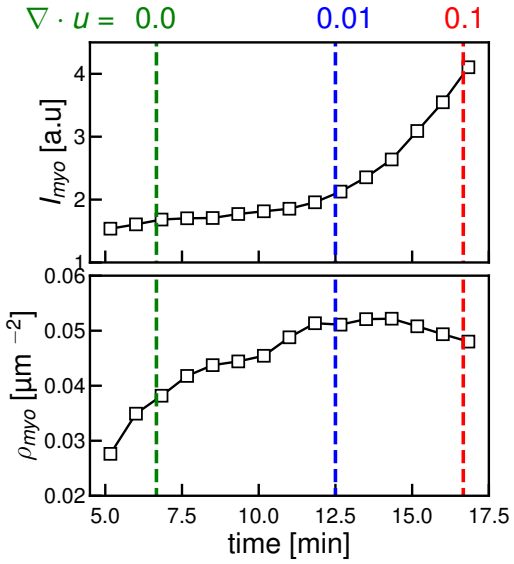

Figure S6: Myosin puncta intensity and density in the active gel studied in figure 2 in the main text. a) Optical intensity of the individual puncta proportional to their sizes. b) density of the myosin puncta over time of observation. The green, blue, and red dashed lines indicate the points taken as characteristic of the gel before contraction, at the onset of contraction, and deep in the contractile regime.

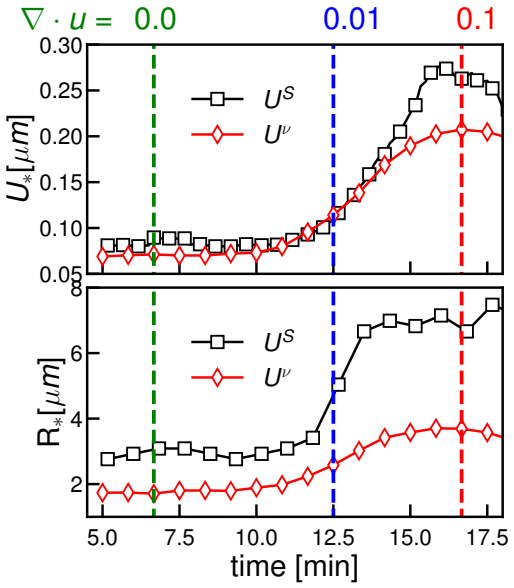

Figure S7: Characteristic length and displacement scales of the active gel studied in figure 2 in the main text. a) Characteristic displacement scales of the shear dipolar mode, U_*^S and vortical mode U_*^ν. b) Characteristic length scales shear dipolar mode, R_*^S and vortical mode R_*^ν corresponding to the displacement scales of U_*^S and $U_*^S\nu$. The green, blue, and red dashed lines indicate the points taken as characteristic of the gel before contraction, at the onset of contraction, and deep in the contractile regime.

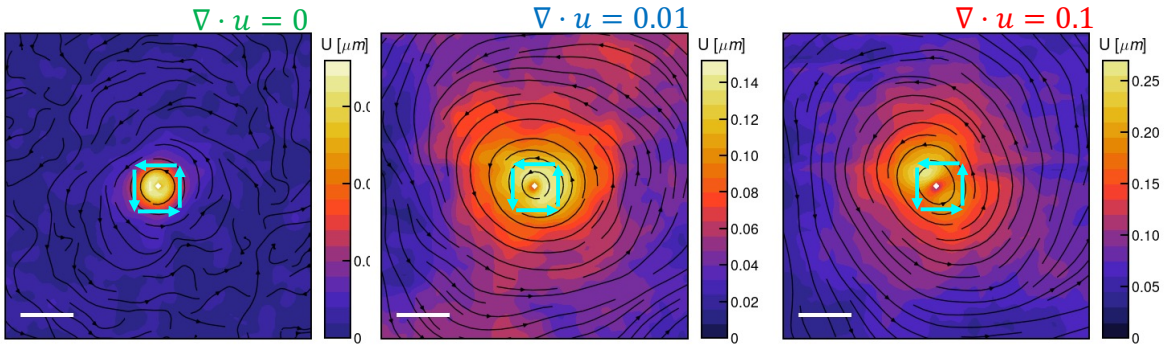

Figure S8: Vortical deformation field of the active gel studied in figure 2 of the main text. Vortical response of the active gel at the stable state with $\nabla \cdot u = 0.0$, at the onset of contraction with $\nabla \cdot u = 0.01$ and deep in the contractile regime with $\nabla \cdot u = 0.1$. Streamlines indicate the direction of the resulting correlation field and color indicates the magnitude; scale bars are 5 µm.

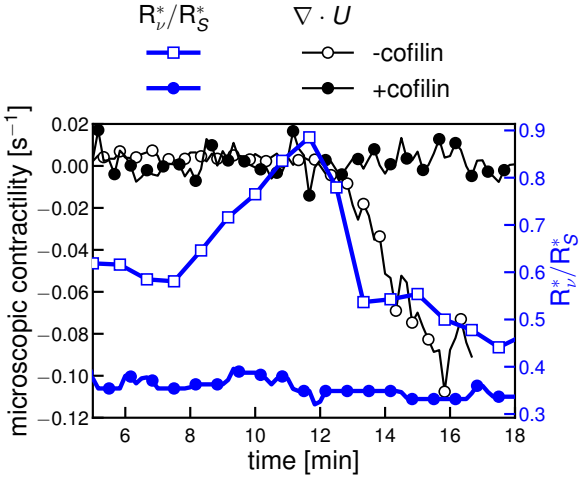

Figure S9: Response functions identify a key difference between contractile and non-contractile active gel. Divergence of the velocity field (black circles) as a function of time for a contractile active gel (-cofilin, open circles) and non-contractile gel (+cofilin, solid circles); ratio of characteristic length scales R^*_ν / R^*_S as a function of time for corresponding systems. Unlike in contractile gel (open square) R^*_ν / R^*_S does not increase in non-contractile gel (closed squares).

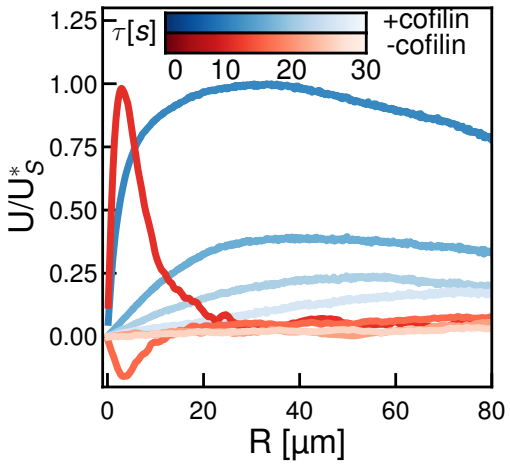

Figure S10: Cofilin ablates the elastic response of an active gel To confirm this interpretation, we compare gels with and without the addition of the actin severing protein cofilin which dissipates elastic stress through filament severing [**?**]. We find that a gel with cofilin never anticorrelates as is consistent with its role in preventing stress buildup in actin networks. The one dimensional shear response U_S as a function of lag time (lighter colors indicate later lag times) for an active gel with (blue) and without (red) the addition of the actin severing protein cofilin.

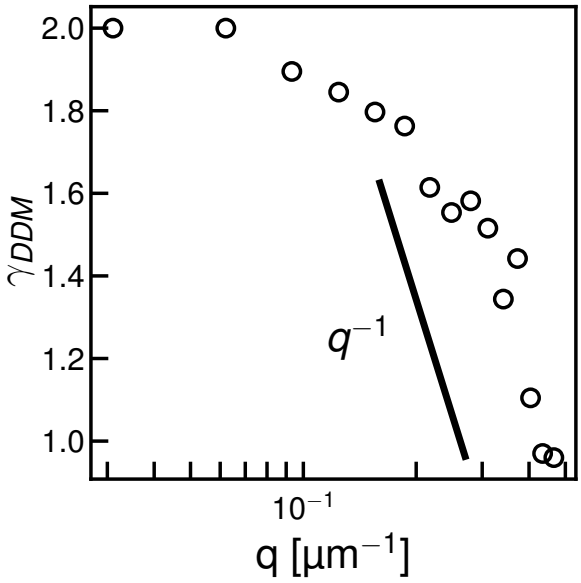

Figure S11: Characteristics factor of image structure function Stretched and compressed exponent of the exponential rise γ_{DDM}, of the image structure functions shown in Fig. 3C obtained by fitting $D(q,\tau)$

.

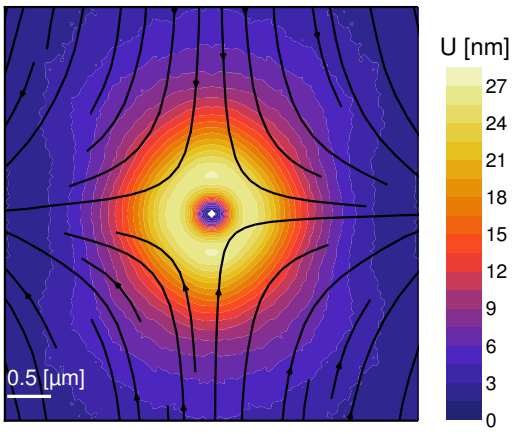

Figure S12: Anisotropic shear dipolar deformation in U2OS cell. Shear dipolar deformation field shown in figure 4C,ii after subtracting linear isotropic deformation field, revealing isolated local deformation field from the global retrograde flow.